Int. J. Solids Structures Vol. 30, No. 4, pp. 463–482, 1993
Printed in Great Britain

0020–7683/93 $5.00+ .00

ON THE LOCALIZATION OF COLLAPSE IN CYLINDRICAL SHELLS UNDER EXTERNAL PRESSURE

J. Y. DYAU and S. KYRIAKIDES
Engineering Mechanics Research Laboratory, Department of Aerospace Engineering and Engineering Mechanics, The University of Texas at Austin, Austin, TX 78712, U.S.A.

(*Received* 2 *June* 1992; *in revised form* 4 *August* 1992)

Abstract—It is well known that long cylindrical shells used in many practical applications involving external pressure loading collapse catastrophically due to a limit load instability. The limit load is due to interaction between geometric nonlinearities and material nonlinearities due to plasticity. This paper addresses the mechanism of collapse triggered by the limit load instability. It is found that following the limit load the collapse quickly localizes to a section of the shell a few diameters long. The deformations and stresses in the region of localization grow with a decreasing overall pressure whereas the rest of the structure remains intact and retains only a small residual effect from the limit load instability as it unloads. However, under favorable conditions the localized collapse triggers an instability which propagates along the length of the shell and has the potential of catastrophically collapsing the whole structure. The characteristics of the localization are studied parametrically through experiment and analysis.

INTRODUCTION

This paper is concerned with the buckling and post-buckling behavior of long, circular, cylindrical shells under external pressure. In particular, we are interested in shells which are thick enough for the plastic characteristics of the material to affect the response of the shell, either from the onset of instability or at least soon after first buckling.

The critical buckling pressure (P_C) for shells which are thin enough to buckle in the elastic range, is given by the classical result [see Levy (1884) for ring case]:

$$P_C = \frac{2E}{(1-\nu^2)}\left(\frac{t}{D}\right)^3, \tag{1}$$

where E and ν are the Young's modulus and Poisson's ratio of the material, D is the diameter and t the wall thickness. Buckling takes the form of ovalization of the cross-section ($n = 2$) which, for a long shell, can be considered to be uniform along the length. Buckling is associated with a drastic loss of stiffness, but the post-buckling response initially maintains a small positive stiffness. However, as the ovalization grows, the combined effect of circumferential bending and membrane stresses can cause yielding of the material. As a result of this additional loss of stiffness a pressure maximum is achieved beyond which a structure under prescribed pressure collapses.

A shell with an initial geometric imperfection corresponding to the buckling mode does not bifurcate but develops a limit load instability which depends strongly on the amplitude of the imperfection [see Kyriakides and Babcock (1981)].

If the shells are thicker, so that buckling occurs after the material yields, then $E/(1-\nu^2)$ in (1) is replaced by the appropriate plastic modulus [see Dubey (1969), Chakraparty (1973) and Ju and Kyriakides (1991)]. First buckling occurs at an increasing load but, with the growth of nontrivial deformations, a limit load instability develops again for the same reasons. The sensitivity of the limit load to initial imperfections is also similar [see Yeh and Kyriakides (1986)].

The negative slope of the primary response (pressure-change in volume) of these structures after the limit load indicates that localized deformations may be energetically preferable to the uniform buckling mode after the pressure maximum. Indeed it will be demonstrated through a combination of experiment and analysis that following the limit

load the collapse process quickly localizes to a length which initially is only a few diameters long. The initial length of localization is governed by the geometric and material characteristics of the structure not unlike the way the length of a neck formed after the load maximum in a uniaxial test on a ductile metal is decided. [A broad discussion of solid and structural problems exhibiting localization can be found in Tvergaard and Needleman (1980, 1984).]

The main objectives of this study were to develop a detailed understanding of the process of localization in this problem and to identify the factors that affect it. These goals were pursued through experimental and numerical efforts conducted in parallel. A shell type analysis of the problem was developed which has the necessary geometric and material nonlinearities and allows for the required axial variation of deformations. The experimental effort involved collapsing a number of shells under carefully controlled conditions. Results from three shells used in the experiments will be used to illustrate the phenomena and to validate the numerical results.

PROBLEM FORMULATION

Motivated by the characteristics of the problem observed in the experiments we consider a circular, cylindrical shell of radius R, wall thickness t and overall length $2L$ as shown in Fig. 1. In the Cartesian system shown (x_i, $i = 1, 3$), planes (x_1, x_2), (x_1, x_3) and (x_2, x_3) are assumed to be planes of symmetry. Thus, only the shaded part of the shell (one eighth) is analysed.

(a) *Kinematics*

Sanders' (1963) nonlinear shell kinematics with the assumption that membrane strains are small are adopted [i.e. the lowest level of approximation suggested by Sanders. See also Koiter (1966) and Niordson (1985)]. Points on the undeformed mid-surface are identified by $(x, R\theta)$. Points on the deformed shell are defined by displacements u, v and w in the axial, circumferential and radial directions. The strain of any point on the shell is given by

$$\varepsilon_{\alpha\beta} = (E_{\alpha\beta} + zK_{\alpha\beta})/(A_\alpha A_\beta)^{1/2}, \tag{2}$$

where $E_{\alpha\beta}$ and $K_{\alpha\beta}$ are the membrane and bending strains, z is along the normal to the mid-surface and $A_1 = 1$, $A_2 \simeq 1 + z/R$. The membrane and bending strains can be related to the metric and curvature tensors as follows:

$$E_{\alpha\beta} = \tfrac{1}{2}(a^1_{\alpha\beta} - a^0_{\alpha\beta}), \quad K_{\alpha\beta} = (b^1_{\alpha\beta} - b^0_{\alpha\beta}), \tag{3}$$

where superscripts 0 and 1 represent the undeformed and deformed configurations respec-

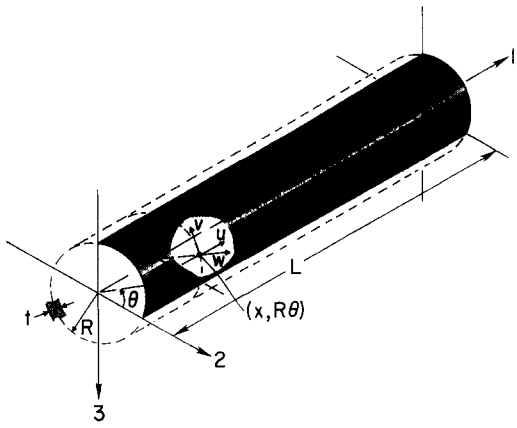

Fig. 1. Geometry of shell analysed.

tively. In terms of the displacements they can be expressed as follows:

$$
\begin{aligned}
E_{xx} &= u_{,x}+\tfrac{1}{2}[u_{,x}^2+v_{,x}^2+w_{,x}^2],\\
E_{\theta\theta} &= \frac{w+v_{,\theta}}{R}+\frac{1}{2}\left(\frac{u_{,\theta}}{R}\right)^2+\frac{1}{2}\left(\frac{v_{,\theta}+w}{R}\right)^2+\frac{1}{2}\left(\frac{w_{,\theta}-v}{R}\right),\\
E_{x\theta} &= \frac{1}{2}\left[\frac{u_{,\theta}}{R}+v_{,x}+u_{,x}\frac{u_{,\theta}}{R}+v_{,x}\frac{(v_{,\theta}+w)}{R}+w_{,x}\frac{(w_{,\theta}-v)}{R}\right],\\
K_{xx} &= -[u_{,xx}N_1+v_{,xx}N_2+w_{,xx}N_3],\\
K_{\theta\theta} &= -\left[\frac{u_{,\theta\theta}}{R^2}N_1+\frac{v_{,\theta\theta}+2w_{,\theta}-v}{R^2}N_2+\frac{w_{,\theta\theta}-2v_{,\theta}-w-R}{R^2}N_3+\frac{1}{R}\right],\\
K_{x\theta} &= -\left[\frac{u_{,x\theta}}{R}N_1+\frac{v_{,x\theta}+w_{,x}}{R}N_2+\frac{w_{,x\theta}-v_{,x}}{R}N_3\right],
\end{aligned}
\tag{4}
$$

where $\mathbf{N}$ is the normal to the deformed mid-surface of the shell given by:

$$
\begin{aligned}
N_1 &\simeq v_{,x}\frac{(w_{,\theta}-v)}{R}-w_{,x}\frac{(w+v_{,\theta})}{R}-w_{,x},\\
N_2 &\simeq u_{,x}\frac{(w_{,\theta}-v)}{R}-w_{,x}\frac{u_{,\theta}}{R}-\frac{w_{,\theta}-v}{R},\\
N_3 &\simeq 1+u_{,x}+\frac{w+v_{,\theta}}{R}+u_{,x}\frac{(w+v_{,\theta})}{R}-v_{,x}\frac{u_{,\theta}}{R}.
\end{aligned}
\tag{5}
$$

Due to the small strain approximation, the square root of the determinant of the metric tensor which appears in the denominator of N_i for finite strains, was neglected. If the shell has initial geometric imperfections then $a^0_{\alpha\beta}$ and $b^0_{\alpha\beta}$ in (3) are replaced by $\bar{a}_{\alpha\beta}$ and $\bar{b}_{\alpha\beta}$ given in the Appendix.

(b) *Constitutive equations*

The inelastic material behavior was modeled through the J_2 flow theory of plasticity with isotropic hardening. With the customary assumption of plane stress the incremental constitutive equations are

$$
\begin{aligned}
\dot{\varepsilon}_{\alpha\beta} &= \frac{1}{E}[(1+\nu)\dot{\sigma}_{\alpha\beta}-\nu\dot{\sigma}_{\gamma\gamma}\delta_{\alpha\beta}]+qs_{\alpha\beta}s_{\gamma\delta}\dot{\sigma}_{\gamma\delta}\\
q &= \begin{cases}\dfrac{3}{4J_2}\left[\dfrac{1}{E_t}-\dfrac{1}{E}\right], & J_2>0,\\ 0, & J_2\leqslant 0,\end{cases}
\end{aligned}
\tag{6}
$$

where $\mathbf{s}=\boldsymbol{\sigma}-\frac{1}{3}\,\mathrm{tr}\,(\boldsymbol{\sigma})\mathbf{I}$, $J_2=\frac{1}{2}\mathbf{s}\cdot\mathbf{s}$, E is the Young's modulus and E_t the tangent modulus. In the numerical simulations that follow the uniaxial stress–strain response was fitted with a Ramberg–Osgood fit (see Table 1) from which

$$
\frac{1}{E_t}-\frac{1}{E}=\frac{3}{7}\frac{n}{E}\left(\frac{3J_2}{\sigma_y^2}\right)^{(n-1)/2}.
\tag{7}
$$

(c) *Principle of virtual work*

Equilibrium was satisfied through the principle of virtual work (PVW) which for pure lateral pressure loading can be written in incremental form as follows:

Table 1. Geometric and material parameters of shells I, II and III

Tube	Material	D in. (mm)	D/t	E msi (GPa)	σ_0 ksi (MPa)	σ_y ksi (MPa)	n	$a_{20} \times 10^3$
I	Al-6061-T6	1.2522 (31.81)	35.0	10.1 (69.6)	44.79 (308.8)	44.5 (306.8)	34	0.52
II	SS-304	1.2555 (31.89)	25.8	29.2 (201.3)	39.8 (274.4)	33.0 (227.5)	9	0.44
III	SS-304	1.3750 (34.93)	18.2	29.3 (202.0)	41.8 (288.2)	37.0 (255.1)	10	0.50

$$\int_0^L \int_0^{\pi/2} \int_{-t/2}^{t/2} (\sigma_{\alpha\beta} + \dot{\sigma}_{\alpha\beta}) \delta\dot{\varepsilon}_{\alpha\beta} A_2 R \, dz \, d\theta \, dx = -(P + \dot{P}) \delta(\Delta\dot{v}), \tag{8}$$

where Δv is the change in the volume of the shell. The form of Δv in (8) appropriate for lateral pressure loading is as follows:

$$\Delta v = \left\{ \int_0^L \int_0^{\pi/2} \left[w + \frac{1}{2}(wu_{,x} - w_{,x}u) + \frac{1}{2R}(w^2 + wv_{,\theta} - vw_{,\theta} + v^2) \right] R \, d\theta \, dx \right\} \tag{9}$$

[see Pearson (1956) and Sewell (1965)]. [A similar formulation which includes finite deformations was used by Jensen (1988) to investigate quasi-static propagation of buckles in such shells.]

(d) *Solution procedure*

The structure was discretized by using the following displacement expansions:

$$u = R\left[c_0 x + \sum_{n=0}^{N} \sum_{m=1}^{M} c_{mn} \sin \frac{m\pi x}{L} \cos 2n\theta \right],$$

$$v = R \sum_{n=1}^{N} \sum_{m=0}^{M} b_{mn} \cos \frac{m\pi x}{L} \sin 2n\theta,$$

$$w = R \sum_{n=0}^{N} \sum_{m=0}^{M} a_{mn} \cos \frac{m\pi x}{L} \cos 2n\theta. \tag{10}$$

The number of expansion terms used varied with the problem solved and, in each case, was decided by numerical convergence tests (typical values, $N \sim 6$ and $M \sim 12$). Integrations were performed by Gaussian quadrature. Typically 6–8 integration points were used through the thickness and $3M$ and $3N$ in the axial and circumferential directions, respectively.

The structure was loaded incrementally by prescribing either the pressure, the deflection $w(0, 0)$ or the change in volume of the shell Δv. A different loading parameter was selected for different stages of the deformation [see Dyau (1992)]. The PVW was suitably extended to accommodate each of the last two loading parameters (can be viewed as constraints).

RESULTS AND DISCUSSION

The mechanisms of collapse will be demonstrated by studying results from three example cases, henceforth referred to as shells I, II and III. Their geometric and material parameters are given in Table 1 and correspond to those of the shells used in the experiments. Shell I was aluminum 6061-T6 and had geometric and material parameters for which buckling was initiated in the elastic range. Shell II was SS-304 with a much lower D/t, so that it buckled in the plastic range. In order to facilitate a direct comparison with the experiments the two shells analysed were loaded by hydrostatic pressure [for this loading

the expression for Δv in (8) and (9) is extended to include terms corresponding to the change in length of the shell (see Dyau, 1992)]. The main objective of this study was to explore the mechanisms of initiation and localization of collapse in long shells. As a result, the shells analysed were selected long enough so that the influence of the boundaries on the response was negligible.

(a) *Initially perfect shell geometry*

We first consider shells which are initially perfectly circular. A set of calculated results for shell I are shown in Fig. 2. The pressure-change in volume response ($P-\Delta v$) is shown in Fig. 2(a) (v_0 is the initial volume enclosed by the shell). The pressure-deflection responses at points C (0, 0) and A ($15D$, 0) are compared in Fig. 2(b) and a sequence of deformed configurations of the generator $(x, 0)$ are shown in Fig. 2(c). The configurations are identified by points in circles on the global $P-\Delta v$ response.

Initially (⓪–①), the shell deforms homogeneously (w = const.). It buckles elastically at $P = P_C$ given in (1). The buckling mode has the form of uniform ovalization of the cross-section and is given by

$$w = a\cos 2\theta \quad \text{and} \quad v = b\sin 2\theta. \tag{11}$$

The initial post-buckling part of the $P-\Delta v$ response has a very small positive slope and the generator $\theta = 0$ is seen to remain straight in configurations ①–④. Thus, the deformation

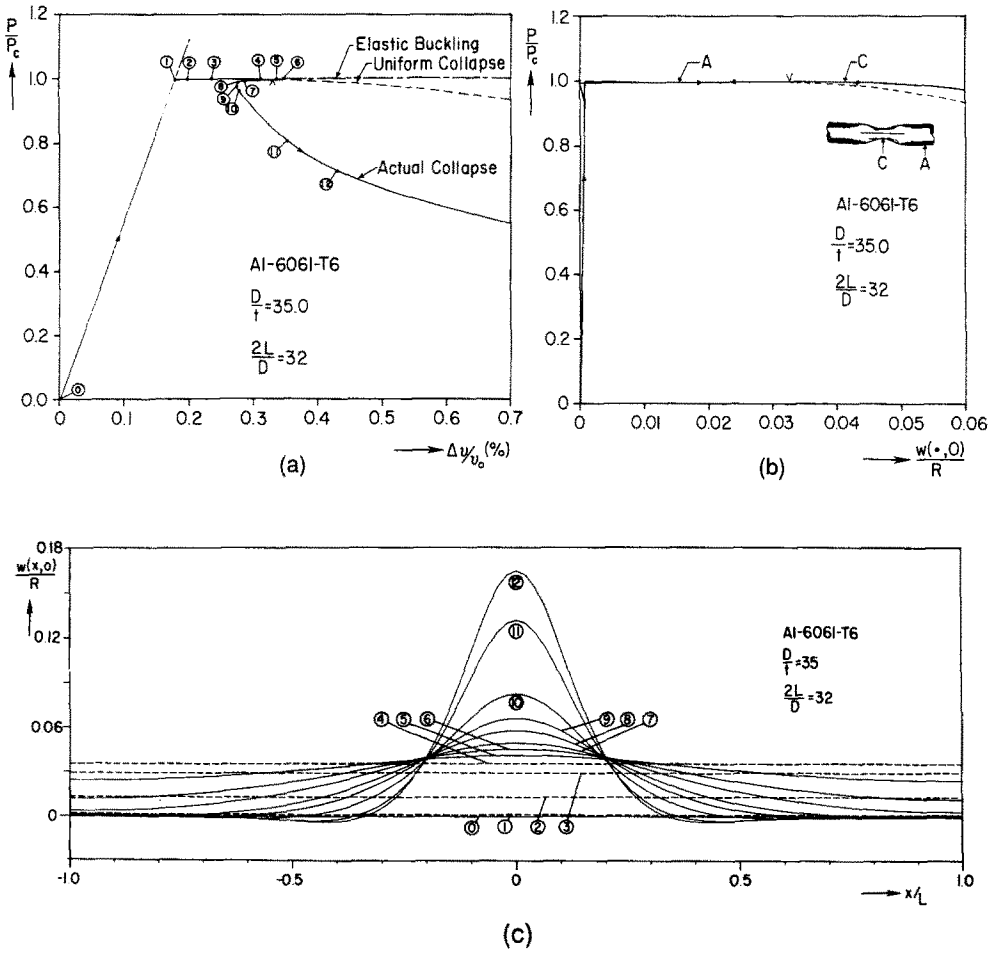

Fig. 2. Numerical simulation of buckling and collapse of shell I. (a) Pressure-change in volume response. (b) Pressure-deflection response at points A and C. (c) Deformed configurations of generator at $\theta = 0$.

is uniform along the length. The significant change in the volume and increase in the deflection at $\theta = 0$ between ① and ④ are due to the growth of uniform ovalization. As long as the material remains elastic the $P-\Delta v$ response maintains a small but positive slope. However, for the parameters of this shell, when the ovalization reaches a critical value the combination of membrane and bending stresses causes yielding of the material at the four points on the cross-section with the largest deflections. This additional reduction in local stiffness induces a limit load instability. In a pressure controlled environment the shell can be expected to collapse catastrophically at the limit load. For this case, this can in essence be assumed to correspond to P_C.

Since the shell deformation remained uniform along the length up to the limit load, this critical condition can be predicted accurately by an analysis in which the deformations are assumed to be axially uniform. Figures 2(a) and 2(b) include results from such an analysis referred to as *uniform collapse*. The negative slope of the $P-\Delta v$ response from the uniform collapse analysis indicates that for long shells, like the ones of interest here, a localized mode of deformation will be energetically preferable. The onset of localized deformation could be identified by a linearized bifurcation analysis. However, like in other similar problems [e.g. see Hill and Hutchinson (1975) and Kyriakides and Chang (1991)], for long shells the first bifurcation point can be expected to coincide with the limit load. Thus, the bifurcation check was avoided in the present study.

In Fig. 2(c) axially varying deformation is first observed in configuration ⑤. At the same time distinct deviation of the actual solution from the corresponding uniform one can be observed in Fig. 2(a). Localization implies growth of deformations and stresses in a section of the shell as the pressure falls. Sections of the shell away from the locally collapsing section undergo unloading. This is illustrated in Fig. 2(b) by comparing the pressure-displacement responses at points C and A. The unloading at point A is essentially elastic and the response follows approximately the same path followed during loading (see also deformed configurations in Fig. 2(c) for $|x/L| > 0.5$). As a result of this, a significant portion of the change in volume induced at points like A during loading is recovered. By contrast, the deflection in the central part of the shell is seen in Fig. 2(b) to grow and as a result its internal volume decreases. In the particular case shown, the increase in volume in the outer half of the shell was larger than the decrease in volume due to localization. Thus, at the early stages of local collapse the shell experiences a net increase in volume which results in the formation of the cusp seen in Fig. 2(a). In the numerical simulation this part of the response was followed by prescribing the deflection $w(0, 0)$. In a volume controlled experiment, on reaching the limit load the structure can be expected to snap dynamically bridging the cusp (i.e. from the limit load to a pressure on the response that corresponds to the same volume change). This type of behavior has also been observed in other problems† governed by limit load instabilities [e.g. see Kyriakides and Chang (1991)].

In the early stages of this deformation process the whole length of the shell is involved. However, the deformation is seen to quickly localize (configurations ⑩–⑫) to a well defined length of approximately 11.5 shell diameters. By this time, the rest of the shell has unloaded to a nearly circular shape. It is interesting to observe that sections of the shell adjacent to the collapsed region undergo reverse ovalization. In this case, the length of these sections is approximately 4 diameters and the maximum amplitude is approximately $7R \times 10^{-3}$. This feature of the deformation has also been observed in experiments.

The length of the localization is governed by local equilibrium considerations and is independent of the overall length of the shell. Changing the shell length does not affect the region undergoing decrease in volume but affects the length which undergoes unloading after the limit load. Thus, the net change in the volume of the shell depends on its overall length. This is illustrated in Fig. 3 in which $P-\Delta v$ responses for shells with lengths of 19.2, 32 and 64 and 960 diameters are compared. The size of the cusp is seen to increase with the shell length. In the longest shell the post limit load response is seen to follow the prebuckling one in reverse until the pressure has dropped by 40–50%.

† Jensen (1986) in his analysis of a similar shell 45 diameters long with fixed ends observed a limited recovery in volume during the initial stages of localization.

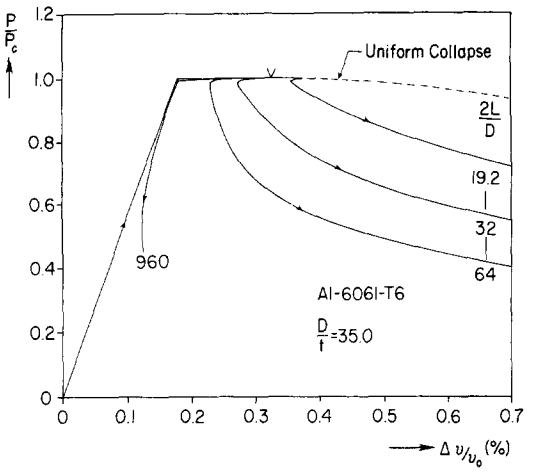

Fig. 3. Pressure-change in volume responses for various shell I lengths.

It is of interest to compare the behavior of shell I with that of shell III which buckles in the plastic range. The $P-\Delta v$ response, the pressure-deflection response at points A and C and a sequence of deflection profiles of the generator at $\theta = 0$ calculated for this shell are shown in Fig. 4. In this case the pressure is normalized by the yield pressure $P_0(2\sigma_0 t/D)$. The initial response (⓪–①) again involves homogeneous deformation which results in relatively small change in the volume enclosed by the shell. Bifurcation occurs in the plastic range at $P_b/P_0 = 0.941$ at an increasing load [see Ju and Kyriakides (1991)]. (For consistency with the post-buckling response, which is calculated by using the J_2 flow theory of plasticity, the bifurcation pressure was also calculated with flow theory moduli. The corresponding value for J_2 deformation theory is $P_b/P_0 = 0.920$.) The buckling mode is again one of uniform ovalization represented by (11). The post-buckling $P-\Delta v$ response initially has positive slope and the ovalization initially grows but remains uniform along the length (①–③). As the bending stresses grow the material modulus is reduced which results in further reduction in the overall stiffness of the structure. This soon results in a limit load instability at $P_L/P_0 = 0.971$. It is of interest to observe that in contrast to the results of shell I which buckled in the elastic range, in this case the change in volume induced to the shell up to the limit load is relatively small. With the downturn in pressure, the deformation again localizes as seen in Fig. 4(c) for configurations ③–⑦. In the process, the central section of the shell undergoes an increase in deformation and stresses, but the rest of the shell "unloads". Since the whole shell had experienced plastic deformations before the limit load the unloading is in essence elastic as seen in Fig. 4(b) for point A; that is, not all of the pre-buckling deformation and volume change is recovered. As a result, the cusp-like behavior observed in the $P-\Delta v$ response of shell I does not occur in this case. In fact, for the shell of length $2L = 29D$ considered here, the volume monotonically decreases during the collapse process. Thus, at least in principle, in this case the post-buckling response could be followed experimentally by volume controlled pressurization. Another interesting difference is that the length of the localized section in shell III is approximately $9D$ as opposed to $11.5D$ for shell I.

The effect of the length of the shells on the $P-\Delta v$ response is illustrated in Fig. 5 in which results for shells with lengths of 29, 58, 87 and 970 shell diameters are compared. Increase in the length of the shell causes a reduction in the initial post-buckling slope of the response which is seen to asymptotically approach a slope equal to that of the initial loading. Thus, even though in this case the cusp-like behavior is not present for longer shells the collapse process again cannot be controlled by prescribing any of the global load or deformation variables of the problem. Control could be achieved by prescribing a monotonically increasing variable in the localization region.

In closing this section we observe that in both cases the limit load instability has

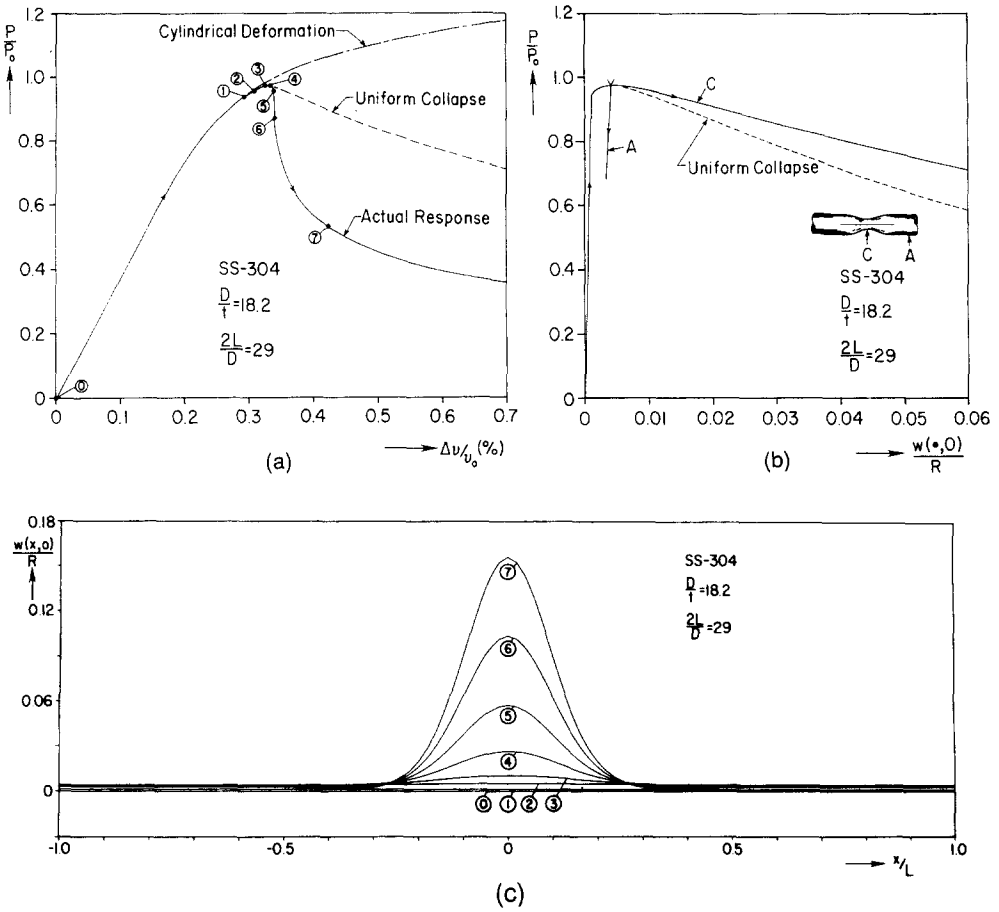

Fig. 4. Numerical simulation of buckling and collapse of shell III. (a) Pressure-change in volume response. (b) Pressure-deflection response at points A and C. (c) Deformed configurations of generator at $\theta = 0$.

resulted from loss of stiffness due to a combination of geometric and material reasons and has resulted in localization of deformation. The cusp-like behavior in the $P-\Delta v$ response is a characteristic of structures which initially buckle in the elastic range.

(b) *Effect of initial geometric imperfections*

From the results presented above, we have seen that geometrically perfect cylinders initially deform and buckle in modes which are uniform along the length. The critical collapse load is the limit pressure after which the deformation was shown to localize. The limit load has been shown in the past to be quite sensitive to geometric imperfections which correspond to the $n = 2$ buckling mode represented by (11) [see Kyriakides and Babcock (1981) and Yeh and Kyriakides (1986)]. It has been observed that collapse-critical tubes and pipes used in practice, often have initial geometric imperfections left by the manufacturing process with long characteristic axial wavelengths [longer than $10D$; see Yeh and Kyriakides (1988)]. As a result, as demonstrated in the references cited above, the collapse pressure can be estimated with good engineering accuracy by using an axially uniform imperfection given by

$$\bar{w} = -a_{2_0} R \cos 2\theta. \tag{12}$$

A conservative prediction is usually obtained by using the maximum value of a_{2_0} measured along the shell length. Table 2 shows a comparison of measured collapse pressures (P_{CO}) and the predicted limit loads for perfect shells and shells with uniform imperfections for the three cases listed in Table 1.

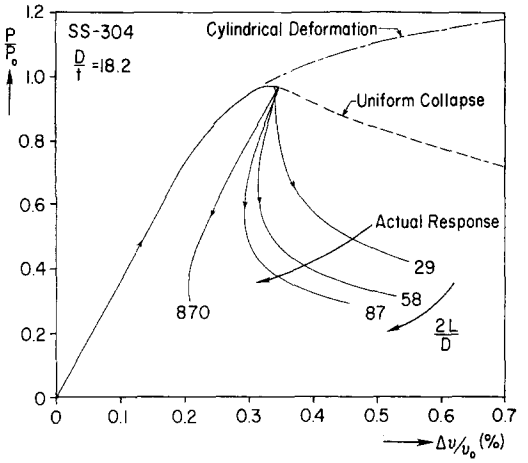

Fig. 5. Pressure-change in volume responses for various shell III lengths.

Results from the current analysis for shells with axially uniform imperfections are shown in Figs 6 and 8 for shells I and III, respectively. In Fig. 6, results for imperfection amplitudes of 0.5 and 3×10^{-3} are compared with those of the perfect case. Like the perfect case, the imperfect shells deform uniformly up to the limit load. Localization takes place after the limit load and the cusp-type behavior is seen to be repeated. In fact, the size of the cusp increases with imperfection amplitude. The reasons for the formation of the cusp are similar to those given for the perfect case, as illustrated by the deformed configurations of the generator $\theta = 0$ shown in Fig. 6(c).

Graphical reproductions of a sequence of collapse configurations for shell I with a small uniform initial imperfection, illustrating the process of instability, are shown in Fig. 7(b) (generated from the solution using a *SunVision* image processing system; deflections amplified five times). The positions of these configurations on the $P-\Delta v$ response are identified in Fig. 7(a). Configuration ① shows the uniform ovalization of the shell just prior to the limit load. Configurations ②–④ illustrate the development of localization.

Figure 8 shows a comparison of results for shell III for the perfect case and for $a_{20} = 3 \times 10^{-3}$. The uniform imperfection lowers the collapse pressure, but the rest of the characteristics of the results are similar to those of the perfect case.

In spite of the general success of the "uniform" imperfection scheme for most design purposes, imperfections induced to long shells during their life (for example, by impact by foreign objects) have distinct axial variation. It is thus also useful to examine the effect of axial length of imperfections on collapse. For long shells no characteristic axial wavelength

Table 2. measured collapse pressures compared with calculated buckling and collapse pressures for shells I, II and III

Shell	P_{CO} psi (bar) Exp.	P_C psi (bar) Anal.	P_{CO} psi (bar) Anal.
I	560 (38.6)	565 (39.0)	557 (38.4)
II	2,498 (168.9)	2,600 (179.3)	2,436 (168.0)
III†	4,360 (300.7)	4,712 (325.0)	4,483 (309.2)

† This shell had a small amount of yield anisotropy which was neglected in the analysis.

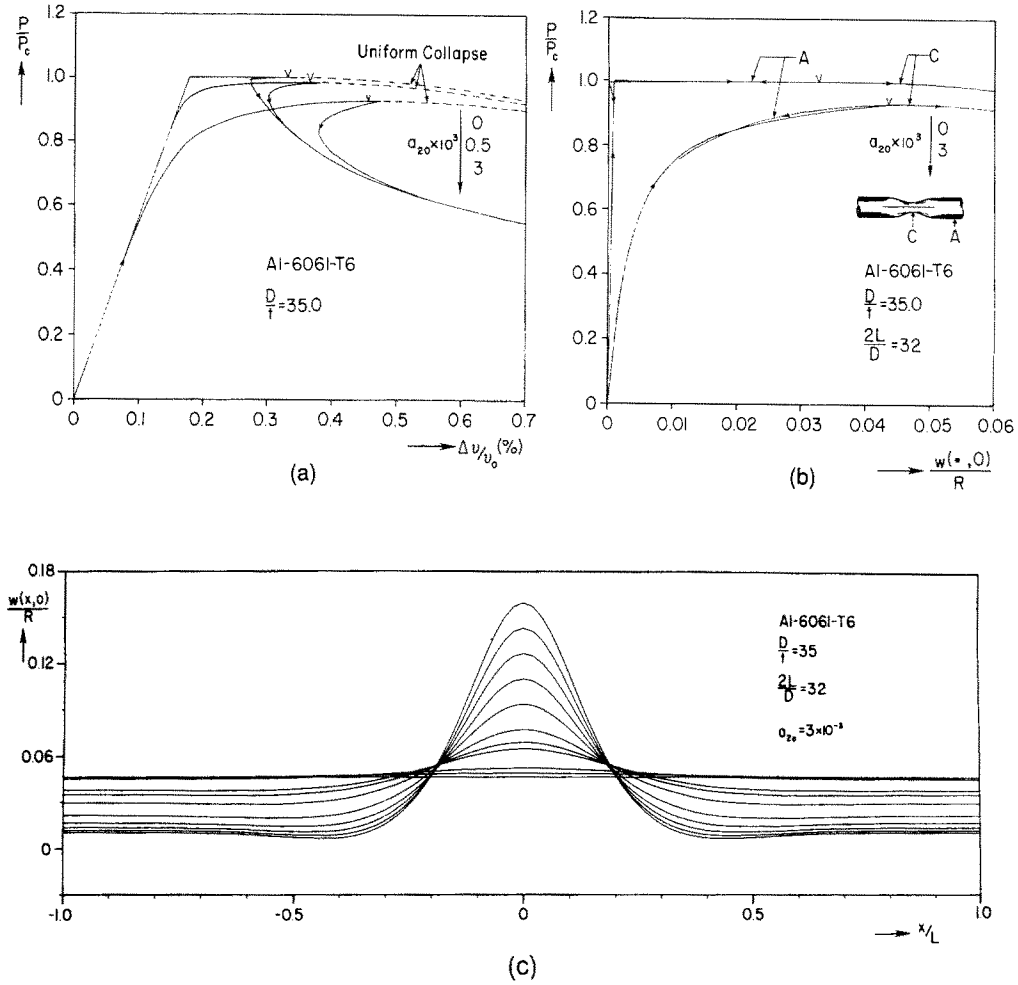

Fig. 6. Numerical simulation of buckling and collapse of shell I with and without initial imperfections which are uniform along the length.

is available to be used as a basis for such an imperfection sensitivity study. On the other hand, the results presented above reveal that, following the limit load, the deformation localizes to a well defined length, as illustrated in Figs 2(c), 4(c), 6(c) and 8(c). Motivated by this observation we adopt an imperfection with a localized component given by

$$\bar{w} = -R\left\{a_{2o} + a_{2i}\exp\left[-\beta\left(\frac{x}{\ell}\right)^2\right]\right\}\cos 2\theta, \tag{13}$$

where 2ℓ is the length of the localized imperfection and β is a constant selected as $e^{-\beta} = 0.01$.

Figure 9 shows a comparison of results from shell I for uniform and localized imperfections with the same amplitude. The length of the imperfection was assumed to be $2\ell = 11.5D$. The calculated limit loads were $0.928P_C$ for the uniform imperfection and $0.959P_C$ for the localized one. A significant difference in the two responses is observed in the neighborhood of the limit load. In the case of the shell with the localized imperfection, pre-buckling deformations are essentially limited to the region of the imperfection. Sections away from the imperfection remain essentially circular and unaffected by the instability as seen in Figs 9(b) and (c). As a result, the overall pre-buckling stiffness of the shell increases as evidenced in Fig. 9(a). In addition, after the limit load, the increase in the volume of the far ends due to unloading is limited, and as a consequence, no cusp develops in the $P-\Delta v$

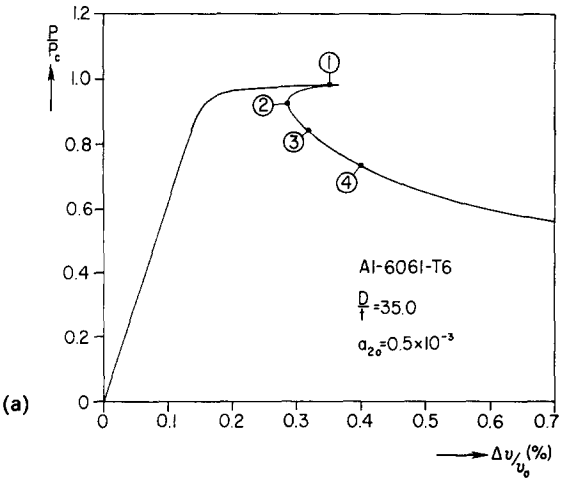

Fig. 7. (a) Calculated pressure-change in volume response of shell I. (b) Sequence of calculated shell configurations demonstrating localization.

Fig. 16. Localized collapse in shell I.

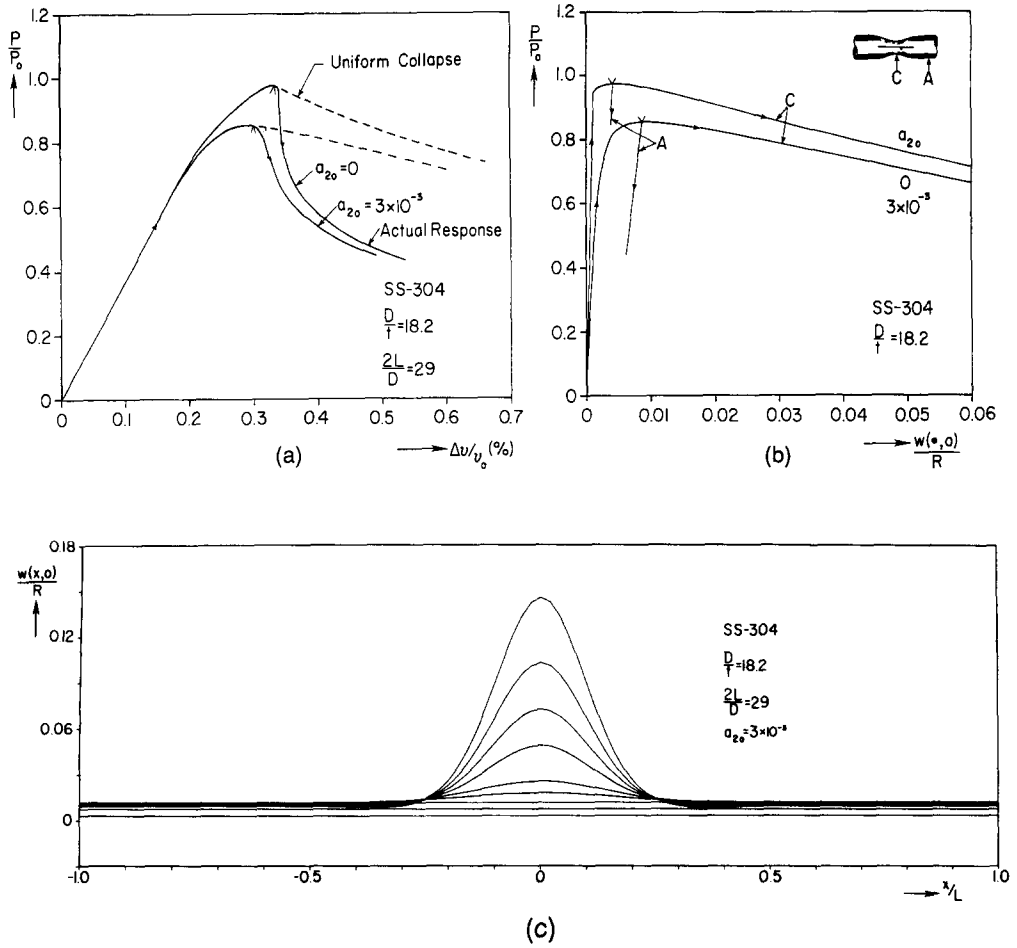

Fig. 8. Numerical simulation of buckling and collapse of shell III with and without initial imperfections which are uniform along the length.

response for this particular shell length. For long shells with such an imperfection the ascending and descending parts of the response will be quite close.

Figure 10 shows a comparison of $P-\Delta v$ responses for the same shell with imperfections with various combinations of a_{2o} and a_{2i} given in the inset. Careful study of the calculated deformed configurations revealed that imperfections with a larger component of the localized imperfection will experience collapse which is more localized. In addition, shells with such imperfections have stiffer pre-buckling responses. On the other hand, if both types of imperfections are present the cusp-like behavior can develop.

Figure 11 shows a similar comparison of results for shell III. In this case, the length of the localized imperfection used was $2\ell = 9D$. The limit load for the uniform imperfection was $0.852P_o$, whereas that for the localized one was $0.887P_o$. The localized imperfection again limits pre-buckling nontrivial deformations to the region of the imperfection. This results in increased overall stiffness of the shell.

A series of collapse calculations were performed for the three shells specified in Table 1 in order to demonstrate the effect of the length of localized imperfections on the collapse pressure. Collapse pressures for $a_{2i} = 0.5\%$ and 2ℓ ranging from approximately $3D$ to $18D$ are shown in Fig. 12. The collapse pressure corresponding to an infinitely long imperfection with the same amplitude is also indicated for each case (axially uniform imperfection). It can be observed that the length of the imperfection can play a significant role on the collapse pressure. Very short imperfections can be considered "benign" whereas long imperfections are "dangerous". It is of practical interest to know at what length a localized imperfection can be considered to be infinitely long. In the discussion above it was proposed that this

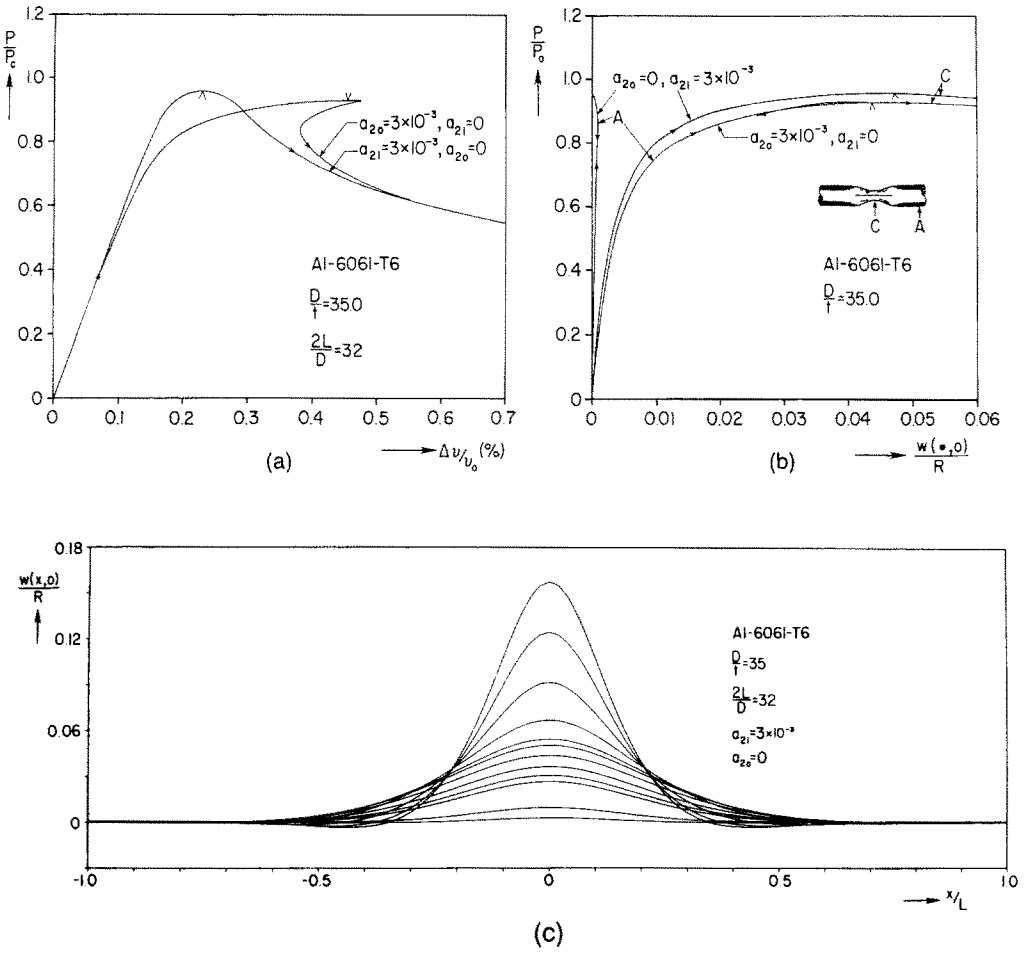

Fig. 9. Comparison of responses for shell I with localized and uniform initial geometric imperfections.

may be related to the characteristic length of localization of the corresponding perfect shell. For shell I this was found to be approximately 11.5 diameters, for shell II 11 diameters and for shell III 9 diameters. The collapse pressures corresponding to these imperfection lengths ($\ell = \ell_L$) and those corresponding to uniform imperfections ($\ell = \infty$) with the same amplitude are as follows:

Shell	P_{CO}/P_C $\ell = \ell_L$	P_{CO}/P_C $\ell = \infty$
I	0.923	0.893
II	0.803	0.750
III	0.872	0.832

The comparison indicates that it is reasonable to assume that imperfections with lengths which exceed the length of localization can be treated as infinitely long. This conclusion was found to be generally true for imperfection amplitudes less than 1%.

(c) *Experimental aspects*

The complex mechanisms of buckling and localization discussed above complicate the experimental investigation of these phenomena. As we have seen from the analysis, it is often not possible to follow (control) the whole response of such structures by prescribing the global load and deformation variables of pressure and volume. In addition, the measured response can also be significantly affected by the stiffness of the test facility [see Babcock

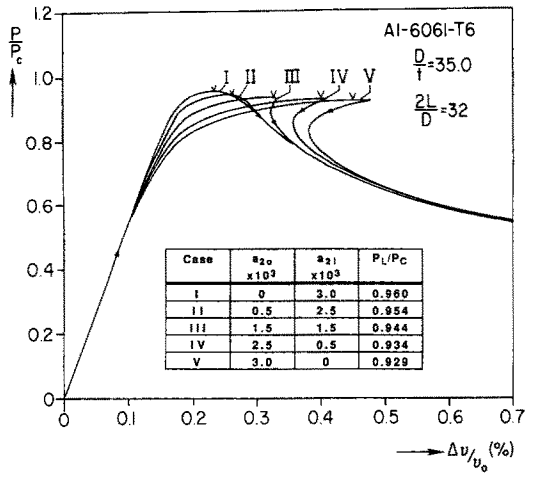

Fig. 10. Comparison of $P-\Delta v$ responses for shell I with various combinations of localized and uniform initial geometric imperfections.

(1967) for a similar study on axially loaded shells]. Some of the experimental limitations are illustrated below.

A select number of collapse experiments on shells I, II and III were conducted in a stiff pressure testing facility shown schematicaly in Fig. 13. The test facility consists of a 4 in. (102 mm) diameter, high strength steel, cylindrical pressure chamber with a capacity of

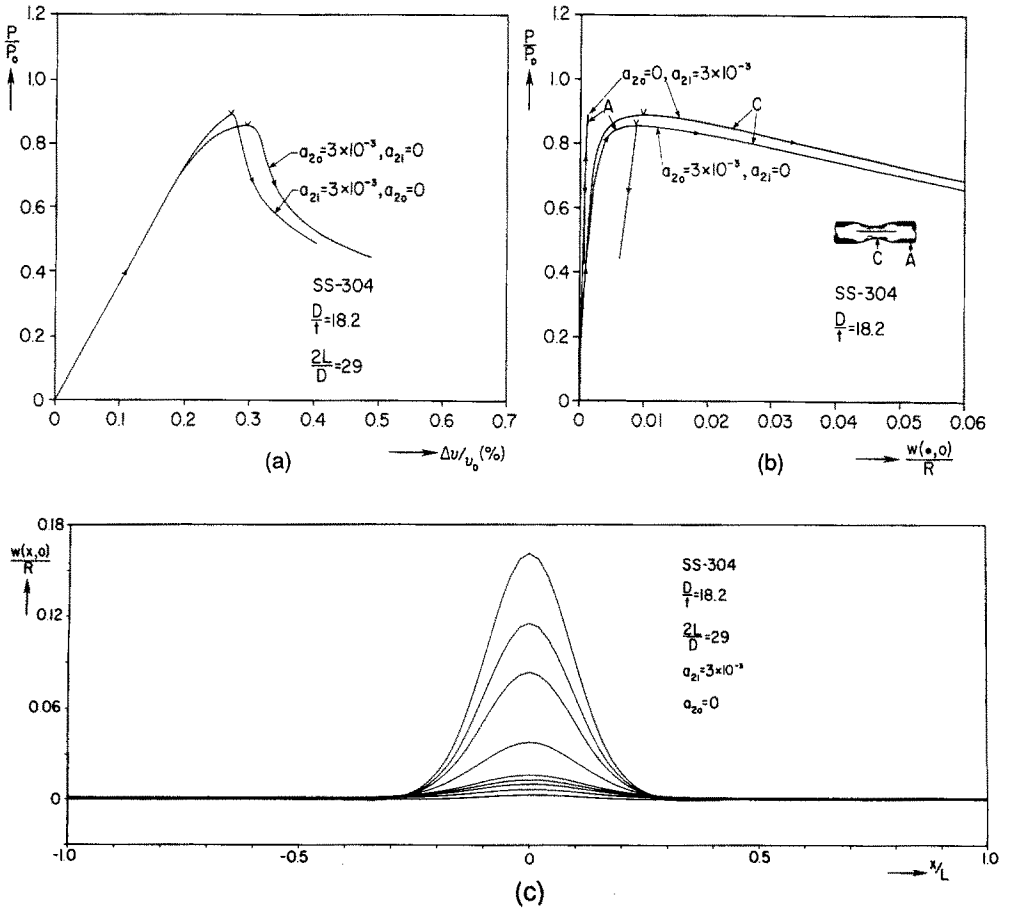

Fig. 11. Comparison of responses for shell III with localized and uniform initial geometric imperfections.

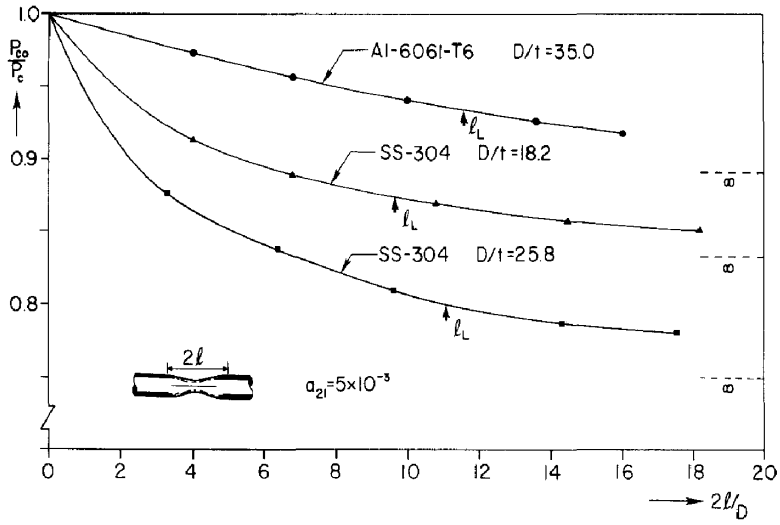

Fig. 12. Calculated collapse pressure as a function of localized imperfection length for fixed imperfection amplitude. Results for shells I, II and III.

10,000 psi (690 bar). The test cavity is 2 in. (51 mm) in diameter and 60 in (1.52 m) long. The pressurizing medium was water and the pressurization was conducted under volume control using an LDC analytical precision metering pump. The tubes tested were closed at the ends with solid plugs (approximately clamped boundary conditions) and were more than 30 tube diameters long.

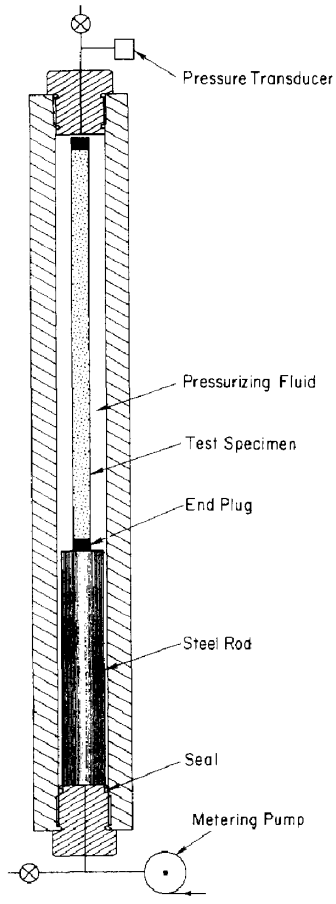

Fig. 13. Schematic of pressure testing facility.

The overall stiffness of the system is affected by the stiffness of the pressure chamber which by design was made to be high but also by the compressibility of the pressurizing fluid. To illustrate this, the pressurization of shells I and III in the test facility was simulated numerically by including the change in volume of the pressure chamber and the pressurizing fluid as described in Dyau (1992). The results are shown in Fig. 14(a, b). It can be observed that by varying the volume of the pressurizing fluid, the stiffness of the response is significantly reduced and the post-buckling response becomes more "unstable". In fact, in the case of shell III; it is essentially impossible to control the post buckling response by prescribing the volume until the pressure drops to the level of the propagation pressure of the shell. In the case of shell I the pressure jump following the limit load could be made to be relatively small by limiting the volume of water in the test chamber. This was achieved by inserting a solid steel rod in the vessel as shown in Fig. 13.

The pressure history recorded in an experiment on shell I is shown in Fig. 15(a). The shell had a length of $30.4D$. The system was pressurized with water at a rate of 0.78 in.^{3} min^{-1} (12.7 ml min^{-1}). Initially the response is seen to be quite linear. Nonlinearity is seen just prior to the pressure maximum at point a. The shell collapsed at a and the pressure dropped suddenly, by approximately 30%, to point b. In the process the shell deformation localized in the fashion described in the analysis. Beyond point b the collapse process could be controlled by prescribing the volume of fluid in the vessel. To illustrate this, at point c a small amount of fluid was released from the chamber. The pressure dropped to d and then recovered following path de. At point e the collapse process continued. The pressure at e was found to be less than 0.5% higher than that at point c. The unloading was repeated at points f and i. In each case the collapse resumed when the pressure recovered to the value at which unloading was initiated. In such an experiment the pressure continues to drop until the walls of the shell in the section of localized collapse touch for the first time. Further pressurization results in spreading (propagation) of the collapse along the length of the shell as discussed in Kyriakides (1992).

As indicated above, beyond point b the collapse process was controlled. In similar experiments to the one described the shell was unloaded at point b and removed from the pressure chamber. The geometric characteristics of the induced localized deformation were measured with micrometers and found to be in very good agreement with those presented in the analysis. A local collapse arrested in this fashion is shown in Fig. 16.

Figure 15(b) shows a numerical simulation approximating the experiment in Fig. 15(a). In this case the change in volume of the test system is used as the history variable rather than time (volume change of test chamber, of fluid and of test specimen). The shell was assumed to have a uniform imperfection with amplitude of $a_{2o} = 0.48 \times 10^{-3}$. Rather than the clamped boundary conditions of the experiment the shell was assumed to be "long". The limit pressure predicted was found to be 0.3% lower than that recorded in the exper-

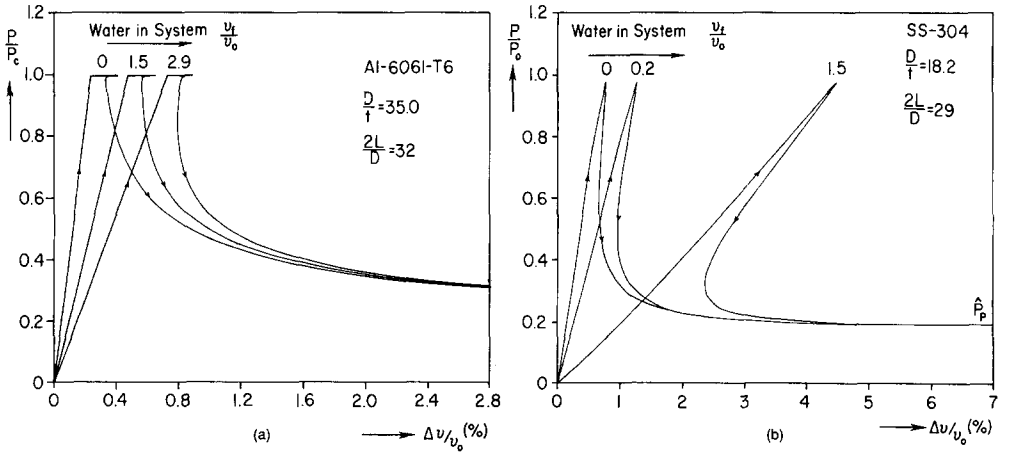

Fig. 14. Pressure versus change in volume of shell and testing system for different initial fluid volumes. (a) Shell I. (b) Shell III.

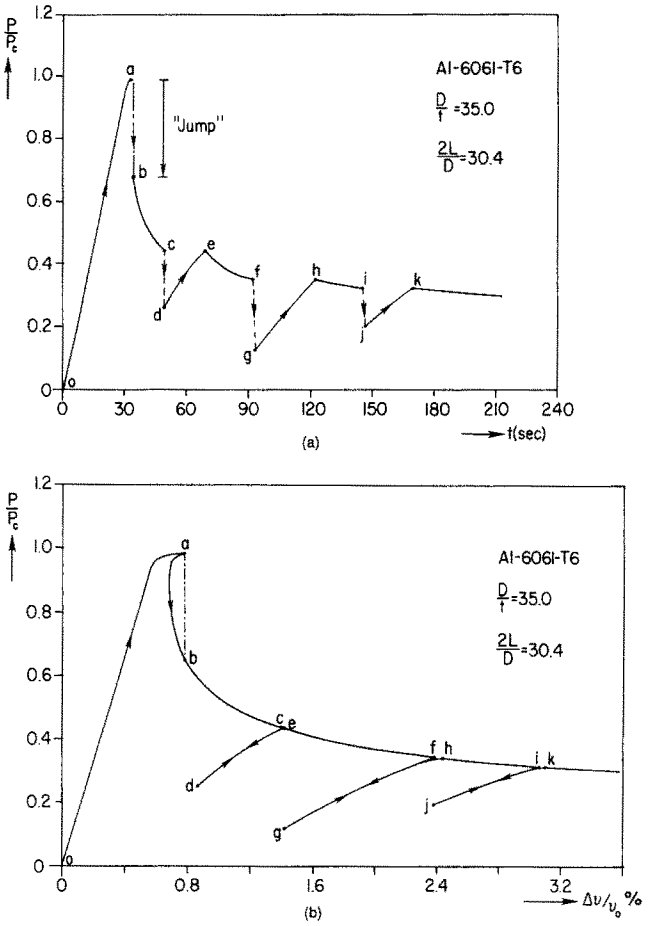

Fig. 15. (a) Pressure history of a collapse experiment using shell I. (b) Numerical simulation of experiment in Fig. 15(a).

iment. The cusp-like behavior following the limit load indicates that in a volume controlled experiment the response can be expected to experience a jump extending from *a* to *b* (assuming that inertial effects are negligible). This jump compares well with that experienced in the experiment shown in Fig. 15(a). As in the experiment, the shell was unloaded at points *c*, *f* and *i* during the collapse process. The paths followed during unloading and reloading are seen in the figure to be almost identical. In each case the collapse process resumed when the pressure returned to the value prior to unloading.

Results from similar calculations on shell I involving unloading after the onset of collapse are shown in Fig. 17. The continuous $P-\Delta v$ response is identified as case I. Case II is the response followed if the shell is unloaded at some point after the localization starts and subsequently reloaded. Like the results shown in Fig. 15(b) we observe that the collapse process resumes when the pressure recovers to the value it had prior to the unloading. The shell has a stable response along *de*, *gh* and *jk*.

In order to further test the effect of localized imperfections on collapse the calculations were repeated but, after unloading to points *c*, the deformed geometry of the shell was captured and used as an initial imperfection in a subsequent analysis. That is, the changes introduced to the material during paths *oabc* were wiped out. The paths followed when this imperfect shell was pressurized are identified as cases III in Fig. 17. Initially the shell deforms elastically along a path which is coincident to that of case II. However cases III are seen to have somewhat lower limit pressure than cases II.

In order to test the appropriateness of the geometric representation of localized imperfections by expression (13) the following comparison was conducted. The length of localization was measured and found to be $2\ell = 11.5D$. Using this length, and the amplitude of

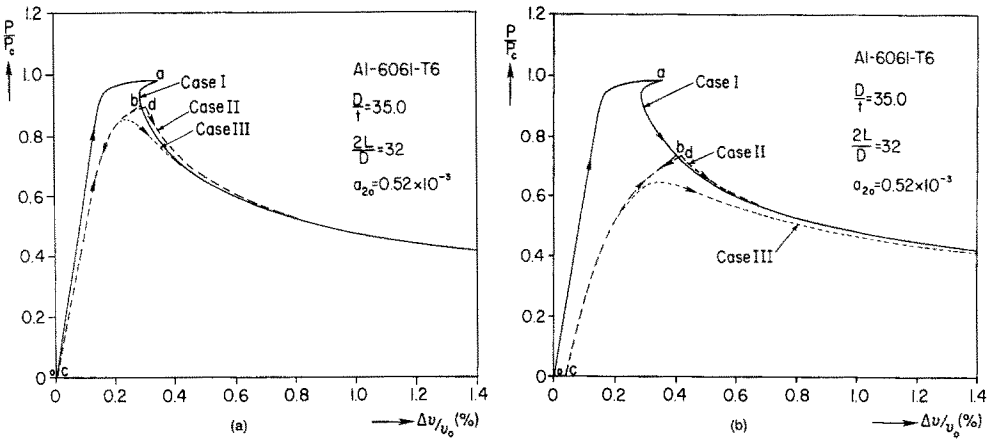

Fig. 17. Comparison of $P-\Delta v$ responses of shell I for three loading cases.

the imperfection formed by unloading along path bc, in eqn (13) the collapse pressure calculated was $0.845P_C$. The collapse pressure calculated when the actual geometry of the localized collapse was used as imperfection [i.e. case III in Fig. 17(a)] was found to be $0.854P_C$. This closeness between the two results was repeated for other imperfection amplitudes. It was thus concluded that expression (13) can be considered to be a good representation of imperfections corresponding to the localized mode of collapse.

CONCLUSIONS

It has been demonstrated that the collapse of long shells loaded by external pressure is local in nature provided that the shells are thick enough to experience plastic deformations during or after buckling. Two categories of behavior were demonstrated. The first involves shells which buckle elastically; the second involves shells which buckle in the plastic range of the material.

The first instability of all such shells takes the form of ovalization which is uniform along the length of the shell. This mode of deformation initially grows stably. However, the extent to which the shell ovalizes uniformly is limited by the development of a pressure maximum in the response. This is due to additional loss of stiffness caused by first yielding in the case of shells in category I and for shells in category II due to further growth of plastic deformations.

Following the limit load, a localized mode of deformation becomes energetically preferable to the uniform mode of collapse. Localization implies that part of the shell experiences growth of deformation and stresses while the rest of it experiences unloading. For shells in the first category, the combined effect results in a cusp in the pressure-volume response. The size of the cusp was shown to depend on the overall length of the shell.

For shells in the second category, the cusp does not develop but, instead, the pressure-volume response for a long shell follows a path approximately parallel to the elastic part of the initial loading.

The localized mode of collapse is quickly concentrated to a section of the shell of the order of 8–12 shell diameters long. The local collapse is arrested when the walls of the shell make contact for the first time. Subsequently, under favorable loading conditions, the collapse can spread (or propagate) along the length of the shell. Thus, localization can be viewed as the process of initiation of a propagating buckle in long shells as discussed in Kyriakides (1992). Thus, for long structures the major danger comes from the propagation of the instability.

The effect of localized imperfections was studied parametrically. It was found that localized imperfections which are short relative to the length of localization have a small effect on the collapse pressure of the shell. On the other hand, imperfections with axial

length of the order of the length of localization were found to reduce the collapse pressure by almost as much as the equivalent axially uniform imperfection.

Acknowledgements—The work reported was conducted with the support of the U.S. Office of Naval Research under contract N00014-91J-1103.

REFERENCES

Babcock, C. D. (1967). The influence of the testing machine on the buckling of cylindrical shells under axial compression. *Int. J. Solids Structures* **3,** 809–817.

Chakraparty, J. (1973). Plastic buckling of cylindrical shells subjected to external pressure. *J. Appl. Math. Phys. (ZAMP)* **24,** 270–280.

Dubey, R. N. (1969). Instabilities in thin elastic–plastic tubes. *Int. J. Solids Structures* **5,** 699–711.

Dyau, J. Y. (1992). Localization and propagation of instabilities in long cylindrical shells under external pressure. Ph.D. Dissertation, Engineering Mechanics, The University of Texas at Austin.

Hill, R. and Hutchinson, J. W. (1975). Bifurcation phenomena in the plain tension test. *J. Mech. Phys. Solids* **23,** 239–264.

Jensen, H. M. (1986). Aksielt forlobende biling af hydrostatisk belastede ror. Ph.D. Dissertation Dept. Solid Mechanics, The Technical University of Denmark.

Jensen, H. M. (1988). Collapse of hydrostatically loaded cylindrical shells. *Int. J. Solids Structures* **24,** 51–64.

Ju, G. T. and Kyriakides, S. (1991). Bifurcation buckling versus limit load instabilities of elastic–plastic tubes under bending and external pressure *ASME J. Offshore Mech. Arctic Engng* **113,** 43–52.

Koiter, W. T. (1966). On the nonlinear theory of thin elastic shells. *Proc. Koninklijke Nederlandse Akademie van Wetenschappen*, Series B, 69, Amsterdam, 1–54.

Kyriakides, S. (1992). Propagating instabilities in structures. In *Advances of Applied Mechanics* (Edited by J. W. Hutchinson and T. Y. Wu), Vol. 30. Academic Press, Boston (to appear).

Kyriakides, S. and Babcock, C. D. (1981). Large deflection collapse analysis of an inelastic inextensional ring under external pressure. *Int. J. Solids Structures* **17,** 981–993.

Kyriakides, S. and Chang, Y.-C. (1991). The initiation and propagation of a localized instability in an inflated elastic tube. *Int. J. Solids Structures* **27,** 1085–111.

Levy, M. (1884). Mémoire sur un nouveau cas intégrable du problème de l'élastique et l'une de ses applications. *J. Math. Pures et Appliquées* **10**(3), 5–42.

Needleman, A. and Tvergaard, V. (1984). Finite element analysis of localization in plasticity. In *Finite Elements: Special Problems in Solid Mechanics* (Edited by J. T. Oden and G. F. Carey), Vol. V. Prentice-Hall, New Jersey.

Niordson, F. J. (1985). *Shell Theory*. North Holland, Amsterdam.

Pearson, C. E. (1956). General theory of elastic stability. *Q. Appl. Math.* **14,** 133–144.

Sanders, J. L. (1963). Nonlinear theories of thin shells. *Q. Appl. Math.* **21,** 21–63.

Sewell, M. J. (1965). On the calculation of potential functions defined on curved boundaries. *Proc. Roy. Soc. London* **A286,** 402–411.

Tvergaard, V. and Needleman, A. (1980). On the localization of buckling patterns. *ASME J. Appl. Mech.* **47,** 613–619.

Yeh, M.-K. and Kyriakides, S. (1986). On the collapse of inelastic thick-walled tubes under external pressure. *ASME J. Energy Resources Technol.* **108,** 35–47.

Yeh, M.-K. and Kyriakides, S. (1988). Collapse of deep water pipelines. *ASME J. Energy Resources Technol.* **110,** 1–11.

APPENDIX

The metric and curvature tensors of a shell with an initial geometric imperfection given by $\bar{w} = \bar{w}(x, \theta)$ are as follows:

$$[\bar{a}_{\alpha\beta}] = \begin{bmatrix} 1+\bar{w}_{,x}^2, & \dfrac{\bar{w}_{,x}\bar{w}_{,\theta}}{R} \\ \dfrac{\bar{w}_{,x}\bar{w}_{,\theta}}{R}, & \left(1+\dfrac{\bar{w}}{R}\right)^2+\left(\dfrac{\bar{w}_{,\theta}}{R}\right)^2 \end{bmatrix}, \tag{A1}$$

$$[\bar{b}_{\alpha\beta}] = \begin{bmatrix} -\bar{w}_{,xx}\left(1+\dfrac{\bar{w}}{R}\right), & -\dfrac{\bar{w}_{,x\theta}}{R}\left(1+\dfrac{\bar{w}}{R}\right)+\dfrac{\bar{w}_{,x}\bar{w}_{,\theta}}{R} \\ -\dfrac{\bar{w}_{,x\theta}}{R}\left(1+\dfrac{\bar{w}}{R}\right)+\dfrac{\bar{w}_{,x}\bar{w}_{,\theta}}{R}, & -\left(\dfrac{\bar{w}_{,\theta\theta}-\bar{w}-R}{R^2}\right)\left(1+\dfrac{\bar{w}}{R}\right)+\dfrac{2\bar{w}_{,\theta}^2}{R^3} \end{bmatrix}. \tag{A2}$$